RESEARCH ARTICLE

DOI: 10.26524/mr1812

Eleyon MATERIALS REPORTS

Spectroscopic investigation of organic phase matchable NLO active oxinium succinate single crystals

B. Mohanbabu [a,*] and R. Bharathikannan[b]

[a] Department of Physics, Sri Shakthi Institute of Engineering and Technology, L & T Bypass Road, Coimbatore – 641 062, Tamil Nadu, India.

[b] Department of Physics, Sri Ramakrishna Mission Vidyalaya College of Arts and Science, Coimbatore – 641 020, Tamil Nadu, India.

***Corresponding Author**
mohanbabuedu@gmail.com
(B. Mohanbabu)
Tel.: +91 9600632570

Received : 01-05-2018
Accepted : 31-05-2018

ABSTRACT: Electro-optic and nonlinear optical (NLO) material, Oxinium Succinate Single crystals of average dimensions 8x6x4 mm3 have been successfully grown by standard slow evaporation technique. The crystallinity of the grown crystals has been analyzed by X-ray diffraction (XRD) curve measurements. Fourier transform infrared (FT-IR) spectroscopic studies were also performed for the identification of different modes present in the compound. The UV-visible absorption and transmittance spectra were recorded for the grown crystal and optical band gap and optical constants are calculated. The relative second harmonic generation (SHG) efficiency was investigated by Kurtz and Perry technique to explore the NLO characteristics of the material. The relative SHG efficiency of the material is 24 times greater than that of KDP and 4 times higher than that of urea. The phase matching property of the crystal is studied through the SHG dependence of average particle sizes. The dielectric study shows that the dielectric constant decreases with increase in frequency. Thermo Gravimetric Analysis (TGA) and Differential Scanning Calorimetry (DSC) studies have been carried out to analysis the thermal properties of grown crystals. The microhardness study was also carried out on the sample.

Keywords: SHG, NLO, Phase matching, Hardness.

1 Introduction

Overwhelming responses of organic molecular engineered materials to the powered laser give promising future for new category of NLO materials. Significant interest in design and development of NLO materials is due to their vital applications in generation of higher harmonic frequencies, frequency mixing, self focusing, electro-optic modulation [1], optical parametric oscillator [2], photorefractivity [3], etc. Such materials have large nonlinear optical coefficients, suitable transparency and excellent comprehensive properties [4–7]. The presence of delocalized π-electrons in organic chromospheres connecting donor and acceptor groups enhance the acentric packing and susceptibility (χ^2) which fulfill the needs of the above fields. Hence they are projected as forefront candidates for fundamental and applied investigations. In this work an attempt has been made to locate a new class of organic NLO crystalline material involving charge transfer mechanism.

In the present investigation, the single crystals of Oxinium Succinate (OS) have been grown for the first time by standard slow evaporation technique. The grown crystals have subjected to powder X-ray diffraction, Fourier transform infrared (FT-IR), UV–vis spectroscopy characterizations. The SHG efficiency of the grown crystals was recorded by Kurtz-Perry method using ND:YAG Q switched laser. The crystallite of various sizes were exposed to the output of ND:YAG laser and the effectiveness of phase matching ability was studied. Differential scanning calorimetry (DSC) and Thermogravimetric analysis (TGA) were also carried out. To unveil the electrical conductivity and mechanical strength of the crystal the dielectric and Vicker's microhardness studies were performed.

2. Experimental

2.1 Material synthesis

The Pure specimens of oxine (8-hydroxyquinaline) and succinic acid were used without further purification for material synthesis. The two reactants were prepared separately in 1:1 molar ratio in acetone:water (1:1) mixture and mixed together. The resulting solution was stirred well for about 30 minutes. The obtained microcrystalline product was filtered off and then purified by repeated recrystallization process in acetone:water (1:1) mixture. The recrystallized compound was used for single crystal growth by the solvent evaporation technique.

2.2 Solubility

Growth of organic crystals with well-defined morphology depends mainly on the solvent used for crystal growth. Solvents offering moderate solubility-temperature gradient for a material and yielding prismatic growth habit will be chosen for growing single crystals of that material. For choosing the most suitable solvent for crystal growth, valuable information can be obtained through solubility test [9]. The different solvents were used to find suitable solvents for OS crystal. The solvents acetone:water (1:1) mixture and chloroform were used. The solubility was measured for different temperatures (30–45 ^{o}C) for acetone:water mixture and chloroform respectively. It was observed that OS exhibits the high positive solubility temperature gradient in acetone:water (1:1) mixture solvent than in chloroform. Hence methanol has been chosen as the solvent for crystal growth. The solubility curves are shown in Figure 1.

2.3 Crystal growth

It is easy to grow single crystals of optical quality of OS using a standard slow evaporation technique. In accordance with the estimated solubility, a saturated solution of OS in acetone:water (1:1) mixture was prepared and stirred well about an hour to dissolve the material completely. The solution was then filtered through a quantitative whatmann 41 grade filter paper to remove the suspended impurities. The beaker containing the filtrate was covered using thin polythene sheet to prevent the evaporation quickly. The perforations were made to regulate the evaporation. The beaker was kept aside unperturbed in an atmosphere most suitable for the growth of single crystals. Proper care was taken to minimize mechanical disturbance and temperature fluctuations. In a normal growth period of 10 days, single crystals of the title material were harvested. Photograph of grown single crystals has been depicted in Figure 2.

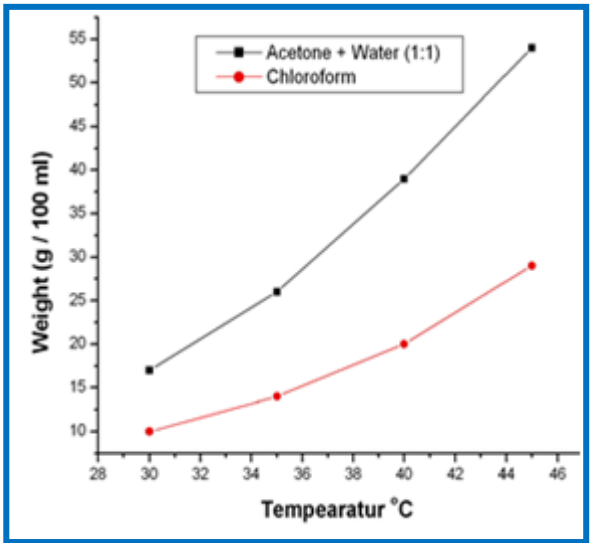

Figure 1 Solubility curves of OS crystal.

Figure 2 Photograph of grown OS single crystals.

3. Results and Discussion

3.1 Powder X-Ray Diffraction Method

X-ray powder diffraction pattern of the OS crystals is shown in figure 3. The sharp and well defined Bragg's peaks at specific 2Θ angles confirm the crystalline nature of the material. X-ray diffraction pattern shows the variation of diffracted intensity with various glancing angles. The peaks in the diffraction pattern are characteristics of the spectrum. These results were in good agreement with the earlier reported results [8]. From XRD spectral data, the microscopic structural parameters grain size (t), dislocation density (ρ) and strain (η) values are

determined from '2θ' values of different peaks. For the major prominent peak (2θ = 14.5197), the microscopic structural parameters are grain size (t) = 54.44 nm, dislocation density (ρ) = 33.7 x 10^{13} lines / m^2 and strain (η) = 1.32 x 10^{-3}.

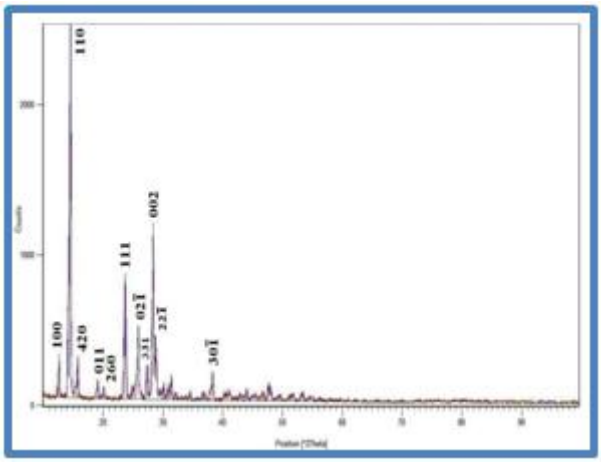

Figure 3 X-ray powder diffraction pattern of the OS crystals.

3.2 FT-IR Analysis

The FT-IR spectrum of OS single crystal was recorded employing Perkin-Elmer FT-IR spectrometer using the KBr pellet technique. The spectrum depicted in the figure 4 shows the presence of characteristic absorption bands due to the varied force constants in the donor and the acceptor species on account of the prevalent charge transfer mechanism. This makes the crystals more ionic than other organic crystals. Normally in an acid base reaction, a proton transfer from the acceptor (acid) to the donor (base) is expected to occur. The band at 3048.48 cm^{-1} is due to the C-H stretching vibration. A peak at 2360.10 cm^{-1} is observed due to O-H vibration. The C–N stretching vibration is observed at 1907.79 cm^{-1}. The absorptions at 1735.50 cm^{-1} is due to C=O stretching vibration of the aromatic ring. The C–N asymmetric stretching vibration is observed at 1578.32 cm^{-1}. The absorptions at 1497.87 cm^{-1} as well as at 1380.26 cm^{-1} are due to C-OH in plane bending vibration. The absorptions at 1285.11 cm^{-1} is due to aromatic C=C stretching vibration of the aromatic ring. The band at 1092.45 cm^{-1} is due to CH2 rocking vibration. Aromatic C-H in-plane and out-plane bending vibration are observed at 1206.31 and 781.36 cm^{-1} respectively. The sharp absorption bands at 741.70 and 711.29 cm^{-1} are attributed to aromatic O-H out-planes bending vibration.

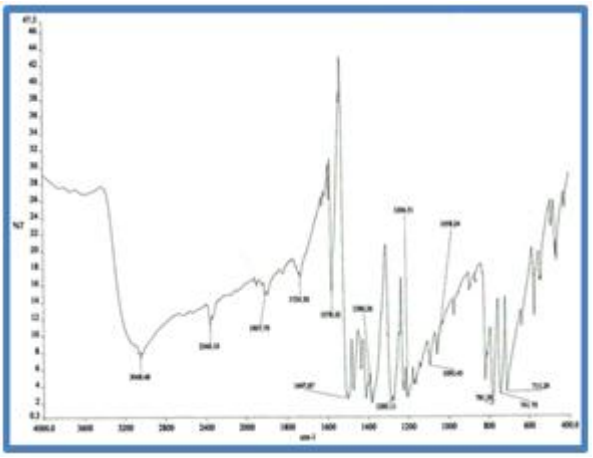

Figure 4 FT-IR spectrum of OS crystal.

3.3 UV-Visible Absorption Spectrum.

The UV-visible absorption spectrum of OS crystal recorded using SYSTRONICS DOUBLE BEAM UV-Vis spectrophotometer in the range 200 – 600 nm. The UV–Visible spectrum gives limited information about the structure of the molecule because the absorption of UV and visible light involves the promotion of the electron in σ and π orbitals from the ground state to higher energy states. The electronic absorption spectrum of the OS crystal is depicted in figure 5. The spectrum reveals that the strong absorption bands attributed to the charge transfer transition and appears around 340 nm. The longer wavelength absorption band arising due to the promotion of an electron from the highest occupied molecular orbital to the lowest unoccupied molecular orbital confirms the formation of charge transfer molecular complex.

3.4 UV-Visible Transmission Spectrum

The transmission spectrum plays a vital role in identifying the potential of a NLO material. A given NLO material can be of utility only if it has a wide transparency window. The UV-visible transmission spectrum of grown OS crystals recorded using SYSTRONICS DOUBLE BEAM UV-Vis spectrophotometer in the range 300 – 800 nm. The spectrum is shown in figure 6. The grown crystal has no absorption beyond the wavelength 370 nm (visible region). Hence this illustrates to know the suitability of the crystal for second harmonic generation and various optical applications [10, 11]. The dependence of optical absorption coefficient with the photon energy helps to

study the band structure and type of transition of electrons [12].

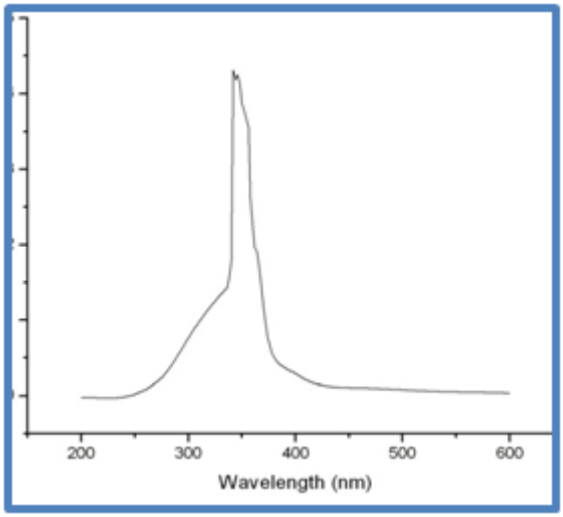

Figure 5 UV-visible absorption spectrum of the OS crystal.

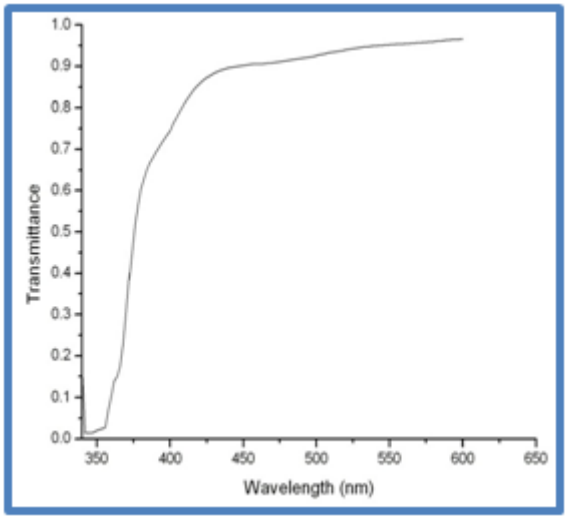

Figure 6 UV-visible transmission spectrum of grown OS crystal.

The optical absorption coefficient (α) was calculated from the transmittance using the following relation,

$$\alpha = -\frac{1}{t}\ln\left(\frac{1}{T}\right) \quad (1)$$

Where T is the transmittance and t is the thickness of the sample. Owing to the indirect band gap, the crystal under study has an absorption coefficient (α) obeying the following relation for high photon energies (hυ),

$$\alpha = \frac{A\left(h\nu - E_g\right)^2}{h\nu} \quad (2)$$

where E_g is optical band gap of the crystal and A is a constant. The plot of variation of $(\alpha h\upsilon)^{1/2}$ vs. hυ is shown in figure 7. E_g is evaluated by the extrapolation of the linear part [13]. The optical band gap energy is found to be 2.51 eV.

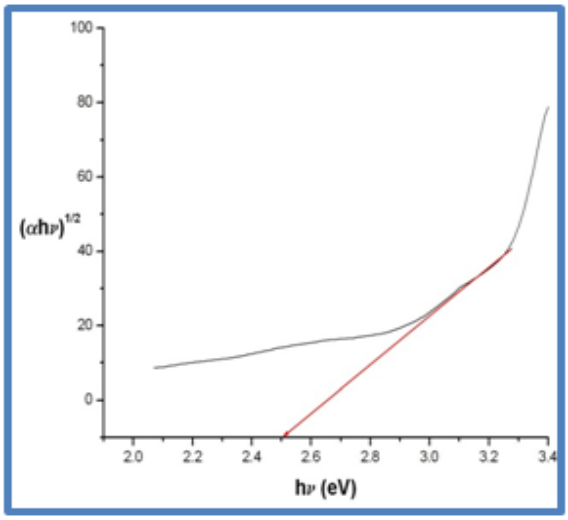

Figure 7 The plot of variation of (αhυ)1/2 vs. hυ of OS crystal.

3.5 Determination of Optical Constants

In optoelectronic application it is important to determine the optical behavior of the materials. Knowledge of a material such as optical band gap and extinction coefficient is quite essential to examine the material's optoelectronic applications [14]. The optical constants are determined from the transmission (T) and reflection (R) spectrum based on the following relations [15].

$$T = \frac{(1-R)^2 \exp(-\alpha t)}{1 - R^2 \exp(-2\alpha t)} \quad (3)$$

Where t is the thickness and α is related to extinction coefficient by

$$K = \frac{\alpha\lambda}{4\pi} \quad (4)$$

The reflectance (R) in terms of the absorption coefficient and refractive index (n) can be derived from the relations

$$R = \frac{1 \pm \sqrt{\left(1 - \exp(-\alpha t) + \exp(\alpha t)\right)}}{1 + \exp(-\alpha t)} \quad (5)$$

$$n = \frac{-(R+1) \pm \sqrt{\left(-3R^2 + 10R - 3\right)}}{2(R-1)} \quad (6)$$

It is clear that both reflectance and extinction coefficient depend on the absorption coefficient. Hence, by tailoring the absorption coefficient, one can get the desired material to fabricate the optoelectronic devices. The refractive index increases with increasing energy. The refractive index (n) is 0.4373 at 550 nm for OS crystal.

3.6 Dielectric Susceptibility

From the optical constants, the electric susceptibility ε_r can be calculated according to the relation [16]

$$\varepsilon_r = \varepsilon_0 + 4\pi\chi_c = n^2 - K^2, \qquad \chi_c = \frac{n^2 - K^2 - \varepsilon_0}{4\pi} \tag{7}$$

where εo is the dielectric constant in the absence of any contribution from free carriers. The value of electric susceptibility λc is 0.01522 at λ = 550 nm. The real part dielectric constant εr and imaginary part dielectric constant εi can be calculated following relations [17]

$$\varepsilon_r = n^2 - K^2 \quad \text{and} \quad \varepsilon_i = 2nK \tag{8}$$

The value of real εr and imaginary εi dielectric constants, at λ = 550 nm are 0.1912 and 1.88 x 10^{-6}, respectively.

3.7 Second Harmonic Generation

The SHG property of as grown OS crystals was examined through modified Kurtz and Perry powder technique [18]. In this method, powdered sample of randomly oriented crystallite particles were tightly packed in a micro-capillary tube. The sample was then subjected to the output of Q-switched Nd:YAG laser emitting a wavelength of 1064 nm with power3.1 mJ/P. The beam was well focused on the sample and the output signal of wavelength 532 nm was generated. This reduction in wavelength of input radiation by half confirms the second harmonic generation property. The green light intensity was registered by a photomultiplier tube and converted into an electrical signal. The signal was then displayed on the oscilloscope screen. The SHG conversion efficiency was computed by the ratio of signal amplitude of the OS sample to that of Urea signal amplitude recorded for the same input power. The SHG efficiency of the grown OS crystal (484 mV) was found to be more than four times to that of urea (112 mV) and twenty four times that of KDP (20 mV).

3.8 Phase Matching Property

To study the phase matching property of the OS crystal, various sizes of the crystallites are subjected to Kurtz-Perry powder technique. Crystals of OS were ground and sieved into distinct particle size ranges (i.e.) below 53, 53–105, 105-149 and above 149 μm. The SHG efficiency of different sizes of crystals was measured. The graph is plotted between average particle size and the second harmonic output values (Fig. 8).

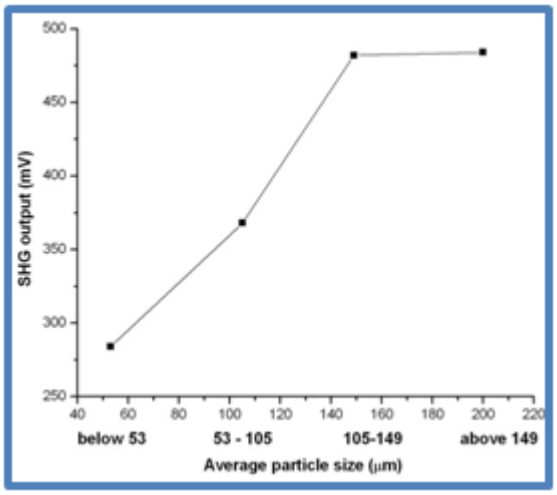

Figure 8 The plot of the SHG output values vs. average particle size of OS crystal.

From the figure, it is observed that the SHG output increases as the particle sizes increase; beyond certain size it attains its upper limit value. It reflects the attainment of the maximum output value of the crystallities. In the case of phase-matchable material it is noted that beyond the coherence length (lc) the output efficiency reaches its limiting value. In this region i.e. >> lc the phase matchable materials have attained their maximum second harmonic intensity independent of particle size [18]. This explains that the grown OS crystal is phase matching material.

3.9 Dielectric Studies

The dielectric study of grown OS single crystal was carried. The capacitance of the sample was measured by varying the frequency from 50Hz to 200KHz. Figure 9 shows the plot of dielectric constant (εr) versus log frequency. The dielectric constant has higher values in the lower frequency region and then it decreases with increasing frequency. The very high values of dielectric constant at low frequencies may be due to the presence of space charge, orientation, electronic, and ionic polarizations. The low value of dielectric constant at higher frequencies may be due to the loss of significance of these polarizations gradually. At high frequency, the

defects no longer have enough time to rearrange in response to the applied voltage; hence the capacitance decreases [19]. In accordance with Miller rule, the lower value of dielectric constant at higher frequencies is a suitable parameter for the enhancement of SHG coefficient [20]. The variation of dielectric loss with log frequency is shown in Figure 10. The characteristic of low dielectric loss at high frequencies for a given sample suggested that the sample possesses enhanced optical quality with lesser defects and this parameter play a vital role for the fabrication of nonlinear optical devices [21].

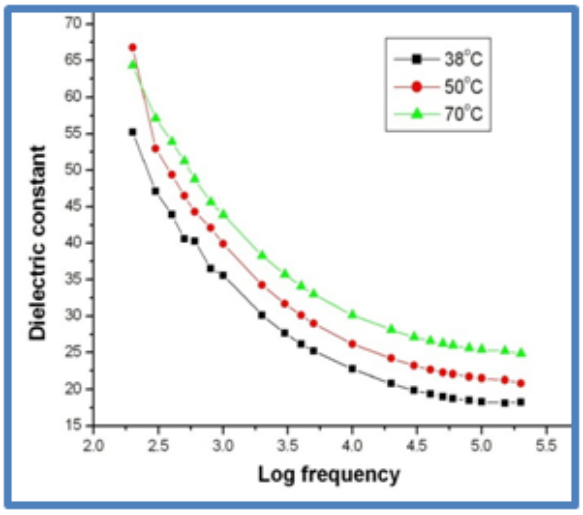

Figure 9 The plot of dielectric constant (εr) vs. log frequency of OS crystal

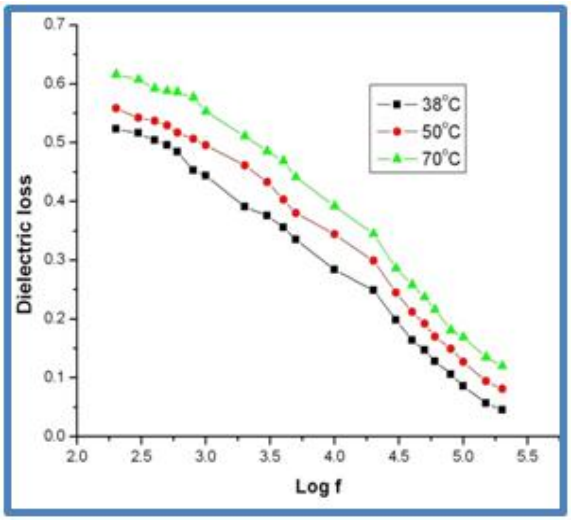

Figure 10 The plot of dielectric loss vs. log frequency of OS crystal.

3.10 Thermal Analysis

Differential Scanning Calorimetry (DSC) and Thermo Gravimetric Analysis (TGA) are carried out at a heating rate of 20 ^{0}C/min in nitrogen gas atmosphere to analyses the thermal property of Oxinium Succinate crystal. Figure 11 illustrates the TGA and DSC curves for the grown OS crystals. From the DSC curve it is seen that the material is structurally stable and there is no phase transition up to 170 ^{o}C. It can be observed that the DSC curve shows the endothermic peak around 170oC related to the melting point of the crystal. The weight loss occurring between 180 and 280 ◦C suggests that the sample decomposes. This is also indicated by the endothermic peak in the DSC curve of the sample at 270 ◦C. It does not decompose at the melting temperature [22]. The TGA curve of the sample coincides with the DSC trace. The sharpness of the endothermic peak shows good degree of crystallinity of the grown crystal.

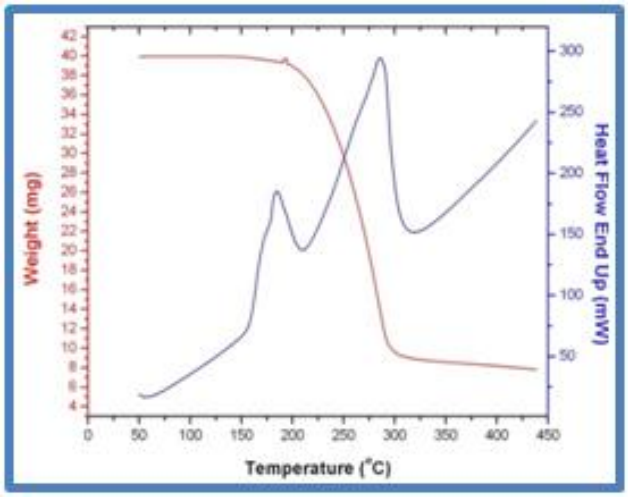

Figure 11 TGA and DSC curves of grown OS crystals

3.11 Microhardness Studies

Microhardness studies have been carried out on OS crystal using a Vickers microhardness tester with a Vickers diamond pyramidal indenter attached to an incident light microscope. The static indentations were made at room temperature with a constant indentation time 10 s for all indentations. The indentation marks were made on the surfaces by varying the load from 25 to 100 g. As micro cracks were developed at higher loads, the maximum applied load was restricted to 100 g only. The Vickers microhardness number Hv of the crystal is calculated using the relation

$$H_V = \frac{1.8544P}{d^2} \quad \text{kg/}\mu\text{m}^2 \qquad (5)$$

where P is the applied load and d the average diagonal length of the indented impressions in millimeter. The Vickers microhardness was evaluated for the OS crystal.

Vickers microhardness profile as a function of the applied loads is illustrated in figure 12

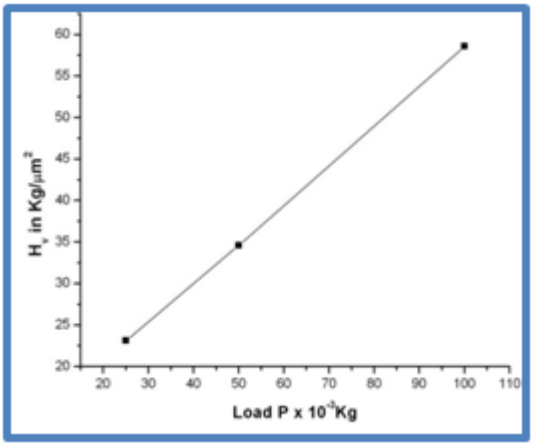

Figure 12 Variation of Vicker microhardness with applied load of OS crystal.

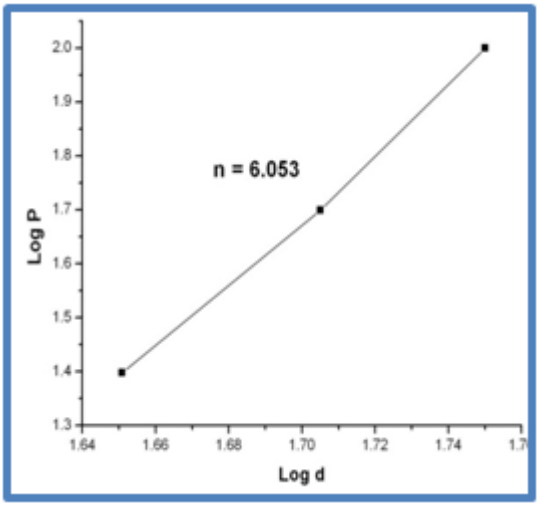

Figure 13 The plot of log d versus log P for OS crystal

It is evident from the plot that the microhardness value of OS increases with increasing load. The value of the work hardening coefficient n was estimated from the plot of log d versus log P, by the least square fit method. According to Onitsch [23], 'n' should be between 1 and 1.6 for hard materials and above 1.6 for softer ones. The plot of log d versus log P for OS crystal is shown in figure 13.

In the present study, n was found to be 6.053 and greater than 1.6, thus confirming that OS was a soft material.

4. Conclusions

The Non Linear optical single crystals of oxinium succinate single crystals were synthesized and grown by adopting slow evaporation technique at room temperature. In X-Ray diffraction pattern, the well defined Bragg peaks at specific 2θ values confirm the crystallinity of the grown crystals. The microscopic structural parameters are calculated for prominent peak values. The FTIR spectra illustrated that the presence of characteristic absorption bands are due to the presence of various functional groups in grown NLO crystal. UV-vis absorption analysis reveals the electron transition around wavelength 340 nm which confirms the formation of charge transfer in grown crystal. The transparency of the grown crystals was studied through UV-Vis transmission spectra. The organic OS crystal showed the transparency beyond 370 nm wavelength (visible) region which is a desire property for various NLO applications. From the transmittance value, the optical band gap was calculated for the grown crystals. The SHG efficiency of OS crystal was 484 mV which is found to be more than four times to that of urea (112 mV) and twenty four times that of KDP (20 mV). The phase matching property of the crystals was studied through the particle size dependence of SHG output illustrates that the grown OS crystals possess phase matching ability. The characteristic of low dielectric loss at high frequencies for grown crystals suggested that the grown crystals possessed enhanced optical quality with lesser defects. From the DSC curve of OS, it was seen that the material was structurally stable and there was no phase transition up to its melting point (170 ^{o}C) crystal. The Vickers microhardness test revealed that the grown crystal was a soft material. Hence the grown OS crystal may be the best candidate for nonlinear optical (NLO) applications and optoelectronic devices.

References

[1] L.R. Dalton, W.H. Steier, B.H. Robinson, C. Zhang, A. Ren, S. Garner, A. Chen, T. Londergan, L. Irwin, B. Carlson, L. Fifield, G. Phelan, C. Kincaid, J. Amend, A. Jen, From molecules to opto-chips: organic electro-optic materials, *Journal of Materials Chemistry*, 9 (1999) 1905-1920.

[2] W.R. Donaldson, C.L. Tang, Urea optical parametric oscillator, *Applied Physics Letters*, 44 (1984) 25.

[3] B. Kippelen, S.R. Marder, E. Hendrickx, J.L. Maldonado, G. Guillemet, B.L. Volodin, D.D. Steele, Y. Enami, Sandalphon, Y.J. Yao, J.F. Wang, H. Rockel, L. Erskine, N. Peyghambarian, Infrared Photorefractive Polymers and Their Applications for Imaging, *Science,* 279 (1998) 54-57.

[4] N. Bloembergen, Nonlinear optics: past, present, and future, *IEEE Journal of Selected Topics in Quantum Electronics*, 6 (2000) 876-880.

[5] B.J. Coe, J.A. Harris, I. Asselberghs, K.Wostyn, K. Clays, A. Persoons, B.S. Brunschwig, S.J. Coles, T. Gelbrich, M.E. Light, M.G. Hursthouse, K. Nakatani, Quadratic Optical Nonlinearities of N-Methyl and N-Aryl Pyridinium Salts, *Advanced Functional Materials*, 5 (2003) 347-357.

[6] S.G. Prabhu, P.M. Rao, Growth and characterization of a promising nonlinear optical organic crystal, *Journal of Crystal Growth*, 210 (2000) 824-827.

[7] S. Manivannan, S. Dhanuskodi, Growth and characterization of a new organic nonlinear optical crystal: semicarbazone of p-dimethylamino benzaldehyde, *Journal of Crystal Growth*, 257 (2003) 305-308.

[8] R. Thirumurugan, B. Babu, K. Anitha, J. Chandrasekaran, Investigation on growth, structure and characterization of succinate salt of 8-hydroxyquinoline: An organic NLO crystal, *Spectrochimica Acta Part A: Molecular and Biomolecular Spectroscopy*, 140 (2015) 44–53.

[9] A. Holden, P. Singer, (1960) Crystals and Crystal Growing, Doubleday and Company Inc, New York.

[10] S. Anie Roshan, C. Joseph, M.A. Ittyachen, Growth and characterization of a new metal-organic crystal: potassium thiourea bromide, *Materials Letters*, 49 (2001) 299-302.

[11] V. Venkataramanan, S. Maheswaran, J.N. Sherwood, H.L. Bhat, Crystal growth and physical characterization of the semiorganic bis(thiourea) cadmium chloride, *Journal of Crystal Growth*, 173 (3-4) (1997) 605-610.

[12] N. Tigau, V. Ciupinaa, G. Prodana, G.I. Rusub, C. Gheorghies, E.Vasilec, Influence of thermal annealing in air on the structural and optical properties of amorphous antimony trisulfide thin film, *Journal of Optoelectronics and Advanced Materials*, 6 (2004) 211-217.

[13] A.K. Chawla, D. Kaur, R. Chandra, Structural and optical characterization of ZnO nanocrystalline films deposited by sputtering, *Optical Materials*, 29 (2007) 995-998.

[14] M.Dongol, Optical absorption and structural properties of as-deposited and thermally annealed As-Te-Ga thin films, *Egyptian Journal of Solids*, 25 (2002) 33-47.

[15] B.L. Zhu, C.S. Xie, D.W. Zeng, W.L. Song, A.H. Wang, Investigation of gas sensitivity of Sb-doped ZnO nanoparticles, *Materials Chemistry and Physics*, 89 (2005) 148-153.

[16] V. Gupta, A. Mansingh, Influence of postdeposition annealing on the structural and optical properties of sputtered zinc oxide film, *Journal of Applied Physics*, 80 (1996) 1063.

[17] M.A. Gaffar, A. Abu El-Fadl, S. Bin Anooz, Influence of strontiumdoping on the indirectbandgap and opticalconstants of ammoniumzincchloridecrystals, *Physica B*, 327 (2003) 43-54.

[18] S.K. Kurtz, T.T. Perry, A Powder Technique for the Evaluation of Nonlinear Optical Materials, *Journal of Applied Physics*, 39 (1968) 3798.

[19] P.W. Zukowski, S.B. Kantorow, D. Maczka, V.F. Stelmakh, Processes of Radiation Defect Interaction and Amorphisation of Silicon at Large Implantation Doses, *Physica Status Solidi A*, 112 (1989) 695-698.

[20] U. Von Hundelshausen, Electrooptic effect and dielectric properties of cadmium-mercury-thiocyanate crystals, *Physics Letters A*, 34 (1971) 405-406

[21] C. Balarew, R. Duhlew, Application of the hard and soft acids and bases concept to explain ligand coordination in double salt structures, *Journal of Solid State Chemistry*, 55 (1984) 1-6.

[22] A. Stanculescu, F. Stanculescu and H. Alexandru, Melt growth and characterization of pure and doped meta-dinitrobenzene crystals, *Journal of Crystal Growth*, 198/199 (1999) 572-577.

[23] E.M. Onitsch, The Present Status of Testing the Hardness of Materials, *Mikroskopie*, 95 (1956) 12-14.

Competing Interests:

The authors declare that they have no competing interests.

About The License